Biosensors and Bioelectronics 79 (2016) 636–643

Contents lists available at ScienceDirect

Biosensors and Bioelectronics

journal homepage: www.elsevier.com/locate/bios

An incremental double-layer capacitance of a planar nano gap and its application in cardiac-troponin T detection

Hsiao-Ting Hsueh [a], Chih-Ting Lin [a,b,*]

[a] Graduate Institute of Biomedical Electronics and Bioinformatics, National Taiwan University, Taipei 106, Taiwan
[b] Graduate Institute of Electronics Engineering, National Taiwan University, Taipei 106, Taiwan

ARTICLE INFO

Article history:
Received 28 September 2015
Received in revised form
24 December 2015
Accepted 29 December 2015
Available online 30 December 2015

Keywords:
Surface potential
Electric double layer capacitance
Cyclic voltammetry
Biosensor
Nano-gap
Coplanar electrode

ABSTRACT

Surface potential is one of the most important properties at solid–liquid interfaces. It can be modulated by the voltage applied on the electrode or by the surface properties. Hence, surface potential is a good indicator for surface modifications, such as biomolecular bindings. In this work, we proposed a planar nano-gap structure for surface-potential difference monitoring. Based on the proposed architecture, the variance of surface-potential difference can be determined by electrical double layer capacitance (EDLC) between the nano-gap electrodes. Using cyclic voltammetry method, in this work, we demonstrated a relationship between surface potential and EDLC by chemically modifying surface properties. Finally, we also showed the proposed planar nano-gap device provides the capability for cardiac-troponin T (cTnT) measurements with co-existed 10 μg/ml BSA interference. The detection dynamic range is from 100 pg/ml to 1 μg/ml. Based on experimental results and extrapolation, the detection limit is less than 100 pg/ml in diluted PBS buffer (0.01X PBS). These results demonstrated the planar nano-gap architecture having potentials on biomolecular detection through monitoring of surface-potential variation.

1. Introduction

At a solid–liquid interface, potential differences between different phases establish a fundamental interfacial characteristic, i.e. electric double layer (EDL) (Bard and Faulkner, 2001), and associated applied properties, e.g. electroosmosis and electrophoresis (Ohshima and Kondo, 1990; Evans and Wennerström, 1999). EDL is resulted from ion redistribution in a liquid phase. This ion redistribution electrically screens solid-surface charges and renders the interface to neutral. As a consequence, EDL is highly related to surface potential and it can be modeled as a capacitor in electrochemical mode (Chapman, 1913). Based on this understanding, various applications can be developed by controlling EDL via external potential fields or surface modifications (Bocquet and Charlaix, 2010; Leroy et al., 2011; Siria et al., 2013). For instance, the change of surface properties can be indicated by measuring the surface potential with different methods, e.g. kelvin probe microscopy and electroosmotic mobility measurement (Jacobs et al., 1998; Gu and Li, 2000; Kirby and Hasselbrink, 2004). Although surface potential is important at the solid–liquid interface, however, most of previous methods are complicated and hard to be implemented as an in-situ monitoring method. Therefore, it is intriguing to develop an innovative method to monitor changes of surface potentials with real-time, low-cost, and easy-operation characteristics.

To address the demand, in this work, we proposed, implemented, and examined an interdigitated nano-gap-electrode device to measure changes of gap EDL capacitance, which is corresponding to surface potential induced by surface modifications. This measurement was achieved by cyclic voltammetry (CV) method. In traditional CV measurements with interdigitated electrodes, generally, the size of electrodes and gaps between electrodes are larger than 10 μm and electrochemical currents mainly flow through bulk solutions. Compared with total EDL effect contributed by electrodes, therefore, the surface-potential effect of the gap between electrodes can be neglected in traditional CV measurements. As the gap size reduces to sub-micro meter, the near surface electrical path, which is different from the traditional electrochemical path through bulk solutions, starts to contribute to the measured electrochemical signal. This near surface electrical path can be affected by surface potentials of the sub-micro gap. And the measured signal includes capacitive difference correlated with the status of surfaces. Since this incremental capacitive change can be measured by cyclic voltammetry (Winter and Brodd, 2004; Simon and Gogotsi, 2008), the change of surface potential can be estimated with the developed nanogap-electrode device.

* Corresponding author at: Graduate Institute of Electronics Engineering, National Taiwan University, Taipei 106, Taiwan.
E-mail address: timlin@ntu.edu.tw (C.-T. Lin).

http://dx.doi.org/10.1016/j.bios.2015.12.105
0956-5663/

Utilizing the developed device, different biochemical reactions, such as chemical modifications and biomolecular bindings, can be monitored because these reactions modulate surface charge from their exposed functional group. To experimentally demonstrate these capabilities, a detection of cardiac-troponin T (cTnT), a major biomarker of myocardial necrosis (Christenson et al., 1998), is examined to have good sensitivity and selectivity. Based on these results, this work successfully developed a novel nanogap metrological architecture for in-situ surface-interface characterizations for different biochemical applications.

2. Devices and methods

2.1. Device fabrication process

The developed nano-gap device was fabricated on a 4 in. silicon wafer with a 300 nm thermally grown silicon dioxide surface. After cleaning the wafer by acetone and isopropyl alcohol, a nano-gap with 200 nm spacing was defined by E-beam lithography (Elionix ELS-7000). The thermal oxide was etched 25 nm by reactive ion etch (RIE). Without removing E-beam photoresist, then, 5 nm Cr and 45 nm Au were evaporated and lifted off to form the nano-gap electrode pattern. Based on this fabrication process, only Au-electrode surface was exposed to surrounded environments (as shown in Supporting information, Fig. S1). The height between the top surface of Au electrode and the nano-gap oxide surface was 30 nm, which corresponds to the length of the antibody used in following experiments.

2.2. Impedance measurement

An electrochemical impedance spectroscopy (EIS) was also performed by SP-150 potentiostat (BioLOGIC Inc.) with low current module and EC-Lab® software package. EIS measurements were set in a frequency ranging from 0.1 Hz to 10 kHz and a sinusoidal amplitude of 10 mV to measure the impedance and capacitance of the electric double layer between the nano-gap devices. These EIS experimental results were measured in a Faraday cage to prohibit electromagnetic interference (EMI). It should be noted that the low current module has a current resolution around 76 femto ampere (10^{-15} A).

2.3. Differential capacitance measurement

Two-electrode cyclic voltammetry (CV) was used to measure the differential capacitance of the nano-gap between the two electrodes. This electrochemical property was characterized by a device parameter analyzer (Agilent B1500A). The voltage operation range was from −0.1 V to 0.1 V. The scan rate was 400 mV/min and step voltage was 2 mV. All the measurement was performed in a Faraday cage to prohibit EMI. We defined capacitance variance ratio $R(\%)=(C'-C_0)/C_0$, where C_0 and C' represents the capacitance before and after treatment respectively. The capacitance is equal to average current divided by scan rate.

2.4. Surface functionalization and antibody immobilization

To have biomolecular sensing experiments based on the developed nano-gap device, the fabricated devices were cleaned by $NH_4OH/H_2O_2/H_2O$ (in 1:1:5 weight ratio, respectively) for 20 min at 70 °C to remove organic residues (Itoh et al., 2011). After rinsed by deionized water, the cleaned devices were immersed in 2% (v/v) aminopropyldimethylmethoxysilane (APDMMS; ACROS Organics) in ethanol for 12 h at room temperature. It should be noted that the whole device including electrodes and gaps were exposed to the following surface modifications. The ethanol residues was remove by 120 °C baking for 20 min and the APDMMS monolayer was cross linked on the SiO_2 surface. At this stage, the amino termination gives positively charged surface in buffer solutions. After measurements, the devices were soaked in 2.5% glutaraldehyde/PBS buffer solution for 1 h at room temperature. Glutaraldehyde forms covalent bonding to APDMMS amino group and transfers surface functional group from amino group to aldehyde group. The aldehyde group makes surface less positively charged than the previous amino termination. To make surface negatively charged, moreover, 10 μg/ml 3-aminobenzoic acid in PBS buffer is injected for 1 h to transfer the aldehyde group to carboxyl group, which is negatively charged. To examine biosensing functionalities of the implemented planar nano-gaped devices, on the other hand, 1 mM 1-Ethyl-3-(3-dimethylaminopropyl)carbodiimide/N-Hydroxysuccinimide (EDC/NHS; Sigma-Aldrich, St. Louis, MO) solution is injected to activate the carboxyl group of the conductive molecule for 20 min so that the carboxyl group can form amide bond with the amine group of antibody. After washing out non-reacted EDC/NHS, 10 μg/ml cTnT antibody (Abcam Inc., Cambridge, MA, USA) in PBS buffer is added and incubated for overnight at 4 °C. Then the device was ready for the cTnT sensing experiment.

2.5. cTnT measurement procedure

For cTnT antigen measurement, a cTnT antibody crosslinked device was treated with diluted PBS buffer (0.01X) containing 10 μg/ml BSA (Sigma-Aldrich, St. Louis, MO). This treatment was used as background till its CV current response becoming stable. This procedure can also be used to block the device and eliminate the interference from non-specific binding. Then, different concentration of cTnT antigens were introduced in the device for detection. After antigen/antibody incubation for 3 min, 0.01XPBS buffer was injected to wash out non-binding antigens. Finally, the devices was electrically probed for CV measurement.

3. Result and discussion

3.1. Device concept validation

Fig. 1(a) shows the optical image of a fabricated nano-gap device (fabrication process can be shown in Supporting information, Fig. S1). The gap width between two electrodes is 200 nm which was defined by E-beam lithography. The electrode height is about 20 nm which is correlated to the length of antibody (Harris et al., 1997; Lasne, 2001). The fundamental concept of the proposed incremental capacitance measurement is based on the nano dimension of the gap and the electrode height. Since the near surface electrical path is highly correlated to the status of surface characteristics, device designs can be utilized to increase the contribution of near surface electrical path comparing to bulk solution path. To experimentally demonstrate basic electrochemical properties, we used electrochemical impedance spectroscopy (EIS) method to measure the fabricated coplanar nano-gap device. In this work, we used two-electrode set-up for electrochemical measurement including impedance and following CV measurement. One electrode acts as a working electrode and the other one acts as a reference/counter electrode. The two-electrode system measures the voltage dropped across the working electrode to electrolyte and electrolyte to the reference/counter electrode. Based on this measurement, the component modulated by the gap-surface potential within the cell can be investigated. In Fig. 1(b), which shows an EIS experimental result, it agrees with previous studies, i.e. the contribution of EDLC mainly presents at low frequency (<100 Hz) and the solution resistance mainly

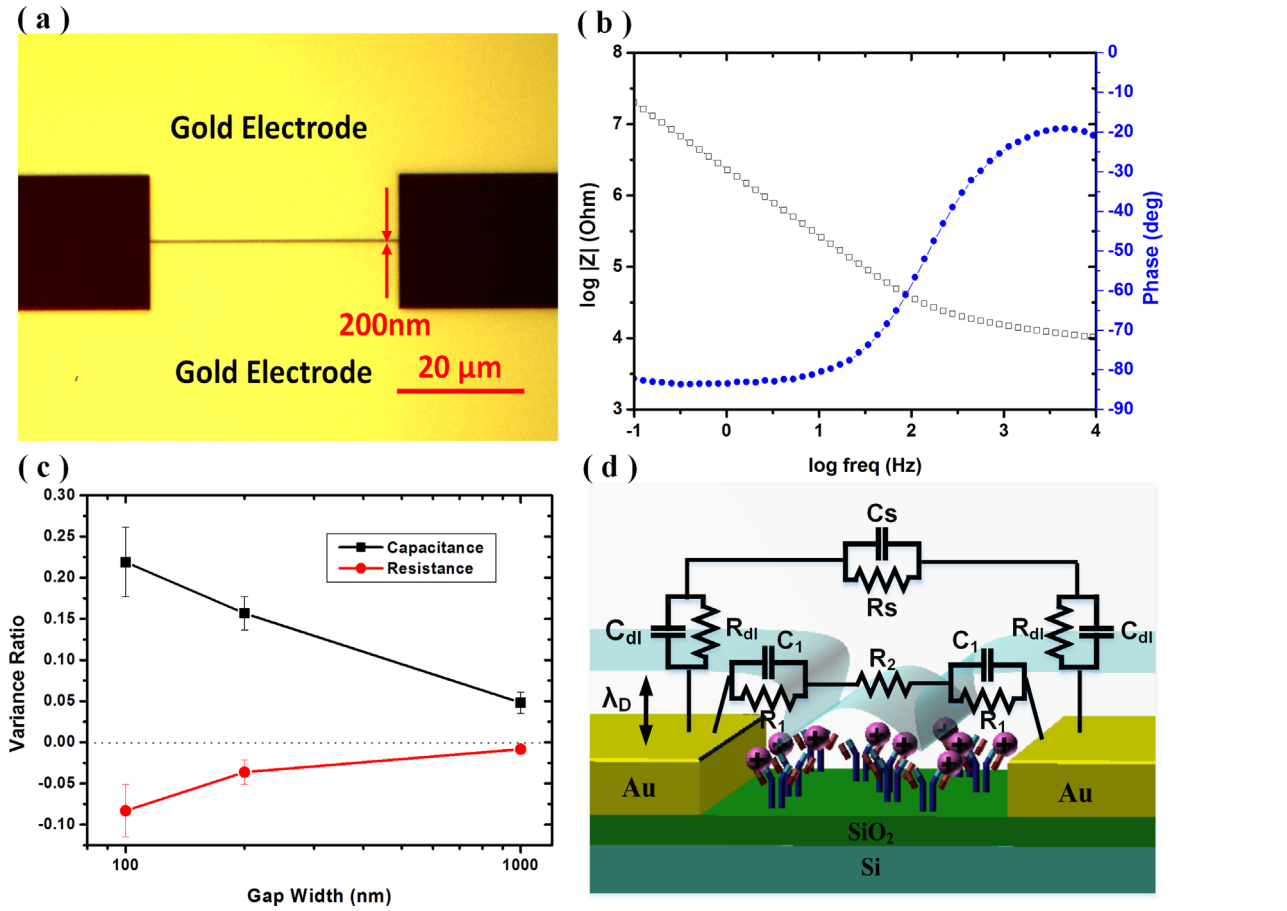

Fig. 1. (a) Optical image of the chip device. The nano-gap between the gold electrodes is 200 nm. (b) The impedance result measured by SP-150. The square line shows the impedance result and the dot line represent the phase result. (c) The result of capacitance and resistance variance ratio versus gap width. This is obtained as the gap surface functional group transfers from aldehyde to carboxyl group in 0.01X PBS buffer. (d) The equivalent circuit model during antigen binding measurement. λ_D represent the Debye screen length. R_{dl}, and C_{dl}, are the electric double layer resistance and capacitance based on Randles model. Rs_l, and C_s represent the liquid resistance and capacitance. For the near-surface electrical path, R_1 and C_1 represent the resistance and capacitance of the sidewall Debye screen length because of the increment of surface ion concentration. R_2 represents the near-surface conductance.

presents at high frequency (> 100 Hz) (Wang and Pilon, 2012). To verify the concept of the near surface contribution in the proposed nano-gap coplanar electrodes, furthermore, Fig. 1(c) represents an experimental relationship of capacitance/resistance variances and different gap widths. The capacitance/resistance variances were induced by different surface functional groups, i.e. changing from aldehyde group (neutral) to carboxyl group (negatively charged). It is clear that the measured capacitance variation ratio between aldehyde-linked and carboxyl-linked surface increases as the gap distance decreases. On the other hand, the resistance variation ratio shows the opposite trend. Based on Fig. 1(b) and (c) results, therefore, we proposed the equivalent circuit model including traditional electrochemical path and proposed near-surface electrical path as shown in Fig. 1(d). In the traditional electrochemical path, which is the upper electrical path in Fig. 1(d), it follows Randles model in bulk solutions and this pathway is dependent to electrode-surface potentials rather than gap-surface potentials (Yang et al., 2004; Valera et al., 2007; Berdat et al., 2008). For the proposed near surface electrical path, which is the lower electrical path in Fig. 1(d), it is closed to the double layer generated by the nano-gap surface potential. The change of surface potential between the nano-gap electrodes induces ion redistribution within the EDL on the top of nano-gap surface, i.e. SiO_2 surface in the developed device. Compared with the bulk-solution path, as a consequence, the near-surface path has a different ion concentration profile induced by the surface potential of the nano-gap surface. This results the fact that the near-surface resistance and the effective capacitance resulted from Debye length of the electrode sidewall are changed as the nano-gap surface potential changes (shown in Fig. 2(a) and (b)) according to Gouy–Chapman Model (Chapman, 1913). Along with the decrease of gap width, therefore, the effect of this near-surface Debye model becomes obvious in the experimental capacitance/resistance variation result as shown in Fig. 1(c). As a consequence, the surface potential between the nano-gap electrodes plays an important role on both of the capacitance and resistance measurement at the proposed nano-gap device.

Based on above discussions, instead of deriving circuit model based on full-span frequency measurement by EIS, CV method was used to be a better method to extract the differential capacitance measurement. It should be noted that the capacitance difference can be obtained by the differential area between two curves of CV measurements. In CV measurements, redox reactions occurring on electrode surfaces contribute undesired current components in differential capacitance measurements. And redox reactions also interfere surface properties including surface potentials. Therefore, redox reactions should be minimized by applying a small operation voltage range, which was set from −100 mV to 100 mV. For the experimental setup, in addition, the nano-gap device and probe station was put in a Faraday cage to shield electromagnetic interference (EMI). As shown in Fig. 2(c), all the CV results exhibited typical quasi rectangular curve shapes and show the electric double layer capacitance behaviors at scan rate of 400 mV/min. Because of the small operation voltage range, no apparent

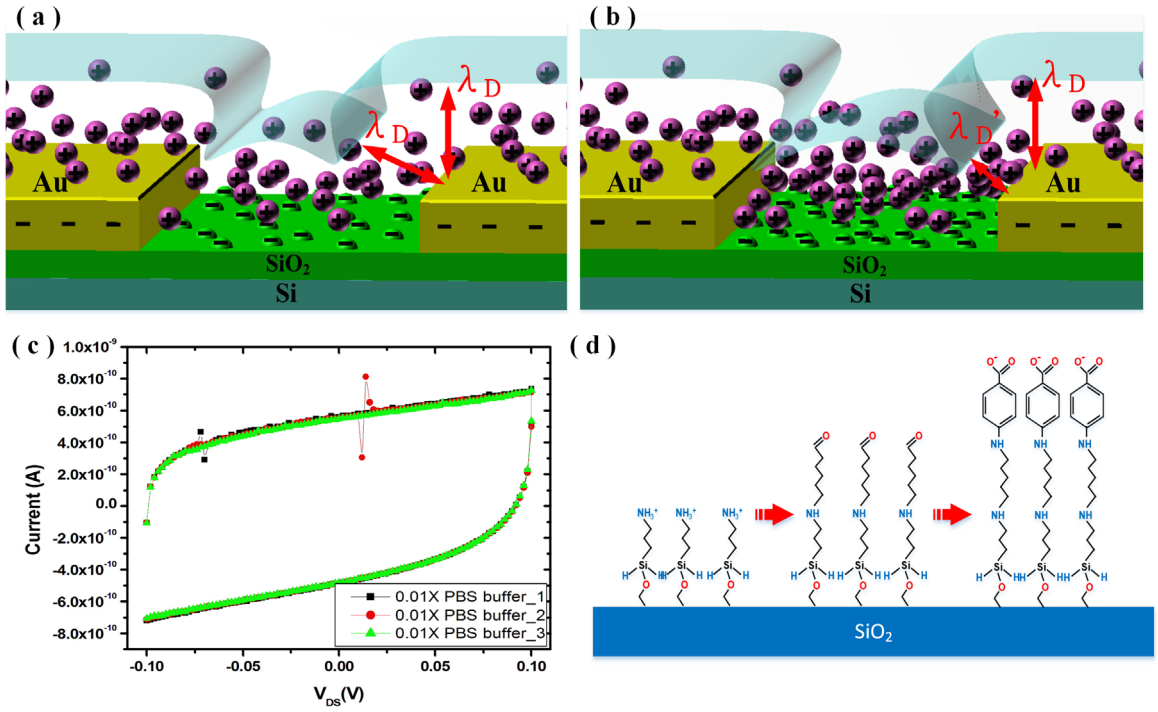

Fig. 2. The schematic of the debye length profile under lower surface potential (a) and higher surface potential (b) λ_D represents the Debye screen length. λ_D' represents the Debye screen length shifting after surface potential shifting. (c) CV measurement curve of the nano-gap device in the diluted PBS buffer (0.01X) at variety time. The scan rate is 400 mV/min. (d) The immobilization process on the silicon dioxide surface.

peak on CV curve profile represents limited redox reactions occurring on the Au electrode surfaces providing the stability of the developed device. To verify the electrochemical stability of the fabricated devices in ionic buffers, a repeated CV measurement in diluted phosphate buffered saline (0.01X PBS) was examined in Fig. 2(c). The average current variations are within few tens of pico ampere (10^{-12} A). The results demonstrate the repeatability and stability during measurement. Because of its good stability, the developed device is capable to detect a small variance of an incremental double-layer capacitance caused by surface potential changes. It should be noted that we used two-electrode experimental setup rather than traditional three-electrode experimental setup. Because bulk solution potential is fixed by a reference electrode, in three-electrode setup, the major voltage drop is across the Debye layer of electrode top surfaces. As a consequence, bulk-solution paths dominant electrochemical reactions and the effect of near-surface paths is diminished.

To further examine the effect of the proposed incremental capacitance can be correlated to surface potential variances by CV measurement, we immobilized different crosslinkers carried different functional groups with different charges in PBS buffer (Fig. 2(d)). Because the upper layer functional group screens the lower layer functional group, different functional groups gives different surface potentials (Taylor et al., 1991a). Aminopropyldimethylmethoxysilane (APDMMS), the first-layer crosslinker, modifies the surface property to amine group (positive charge in PBS buffer). The reason to use APDMMS is that it forms a denser monolayer on SiO_2 surfaces than 3-aminopropyltriethoxysilane (APTES) does (Salmio and Brühwiler, 2007). Glutaraldehyde, the second-layer crosslinker, results in the surface property from amine group to aldehyde group (neutral charge in PBS buffer). Then 3-aminobenzoic acid, the third-layer crosslinker, changes the surface property from aldehyde group to carboxyl group (negative charge in PBS buffer). Fig. 3(a) shows an experimental CV result of a glutaraldehyde immobilized process. The aldehyde group of glutaraldehyde brings less charges than the amine group of APDMMS. In other words, the surface charge density was reduced via glutaraldehyde cross linking. When the glutaraldehyde immobilized on the APDMMS, the surface charge decreased gradually during cross-linking reactions and the capacitance measurement shows the corresponding result as illustrated in Fig. 3(b). In Fig. 3(b), the *y*-axis represents the capacitance variance ratio compared to the APDMMS result at zero voltage. Based on this experimental observation, it can be correlated the fact that aldehyde amine condensing reactions have become equilibrium state after 60 min. For the next step, 3-aminobenzoic acid was used to exchange the aldehyde-terminated surface and resulted in the carboxyl modification on the surface. Fig. 3(c) shows an experimental CV data of a 3-aminobenzoic acid immobilization process. Because of higher electronegativity of carboxyl group than that of aldehyde group, carboxyl group carries more charges than aldehyde group does. The total surface charge within the nano-gap increases gradually during this immobilization process and causes the capacitance raise shown as Fig. 3(d). It should be noted that the capacitance variation was obtained based on the difference to last-step aldehyde surface. As a consequence, it is obvious both amine group and carboxyl group lead to the increase of the capacitance. This phenomenon indicates that charge quantity rather than charge polarity affects the capacitance detection between nano-gap electrodes. In other words, surface potential difference is the key factor of this CV measurement. These experiments show the capacitance variance in CV measurements can be correlated to the surface potential variance within the nano-gap electrode. In addition, these experiments also demonstrate the capability of in-situ monitoring of surface potential changes induced by chemical modifications or biomolecular bindings.

3.2. Surface modification examination

Above phenomenon provides an innovative method to have in-situ surface potential monitoring. To demonstrate one of its applications, in this work, a biomolecular detection is implemented

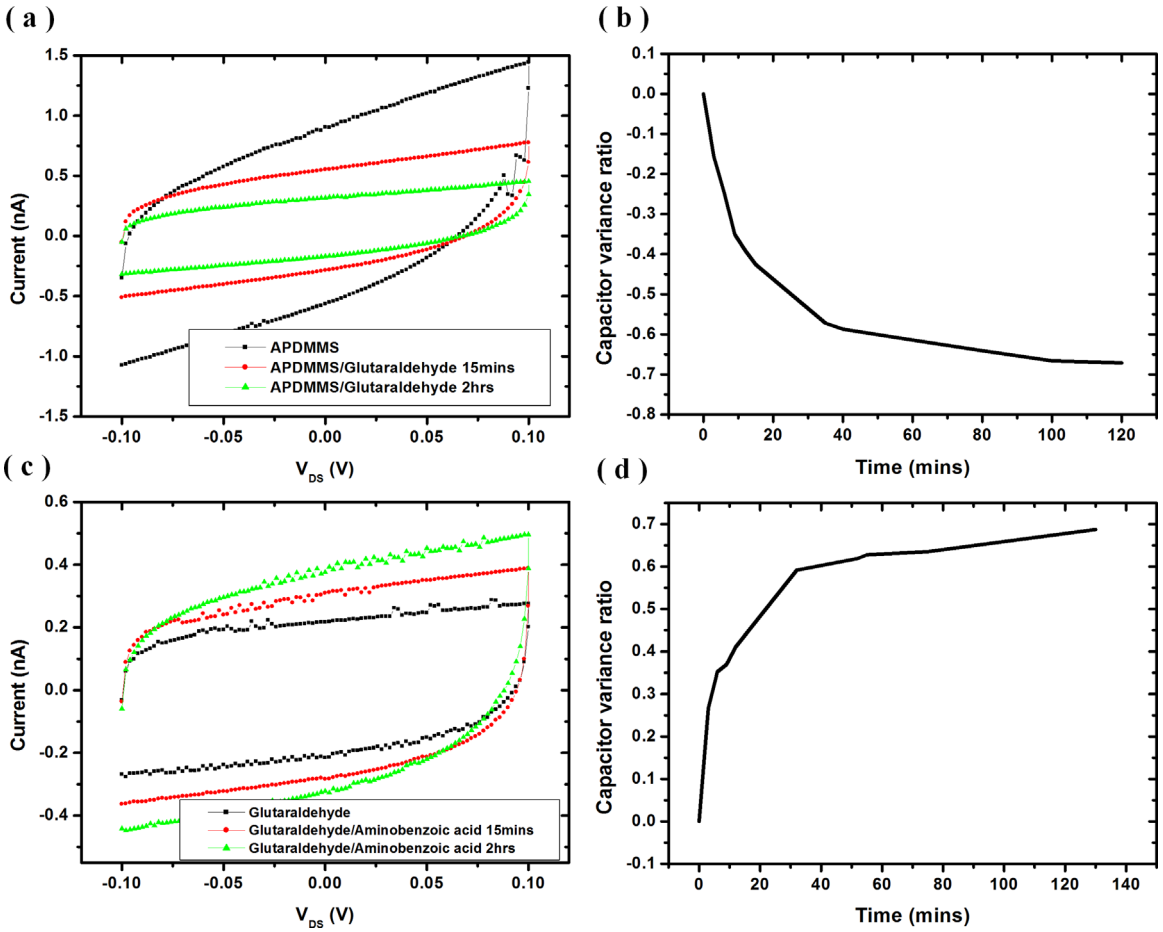

Fig. 3. The CV curves and capacitor variance ratio under different functional group modification. (a) The CV curves response as the glutaraldehyde immobilizing on the APDMMS monolayer surface. (b) The temporal response of the capacitance variation ratio during glutaraldehyde immobilization process. (c) The CV curves response as the 3-aminobenzoic acid immobilizing on the glutaraldehyde monolayer surface. (d) The temporal response of the capacitance variation ratio during 3-aminobenzoic acid immobilization process.

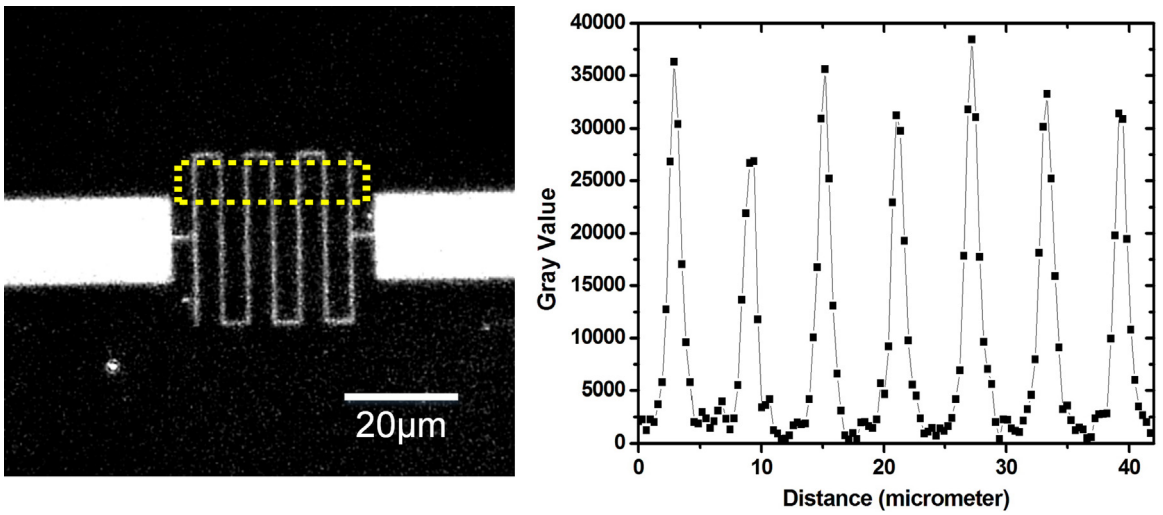

Fig. 4. (a) The fluorescence result of nano-gap device after antibody immobilization. (b) The gray value result from the dash square in Fig. 4(a).

because biomolecules are charged particles. It must be addressed that the fundamental mechanism of the proposed incremental capacitance measurement in nano-gap device is different from traditional electrochemical impedance or capacitance analyses. Traditional electrochemical biomolecular detections are achieved by using fabrication (Taylor et al., 1991b) or immobilization processes (Mirsky et al., 1997; Radke and Alocilja, 2005) to coat target molecules on the top of electrodes. The coated molecules function as insulators on electrode surfaces. By measuring the impedance change induced by bio-recognition or other reaction processes, these measurements provide the ability to function as a biomolecular sensor. As a consequence, these kinds of impedance analyses have a critical drawback that coating molecules should be uniform to perform as an ideal capacitor. The detection signal-to-

noise ratio is deteriorated as the coating layer is not distributed evenly on the top of electrode surfaces (Gu and Li, 2000). In this work, on the contrary, the crosslinker or surface coating molecules are immobilized on the dielectric surface between nano-gap electrodes rather than on the top of electrode surfaces. The measured electrical element is the integral of surface charges, which can be modulated by the surface potential between nano-gap electrodes. As a consequence, the uniformity problem of cross-linkers or coating molecules on the nano-gap can be mitigated and the change of surface potential can be measured directly.

Since the proposed mechanism is used to monitor the surface potential change between nano-gap electrodes rather than on the top of electrode surfaces, non-specific binding biomolecules on the top surface of electrode might introduce undesired capacitance changes. To verify the position of biomolecular immobilizations, fluorescence was used to tag the antibody. Fig. 4(a) shows a fluorescence result after the antibody immobilization. The black part is gold electrode area, where few antibodies non-specifically bind on it. And high fluorescent intensity regions are the gap between gold electrodes. Fig. 4(b) shows the fluorescent intensity from the marked region (yellow dash line) in Fig. 4(a). The fluorescence result, about 10 times in intensity difference, indicates the antibody immobilization process has high selectivity between gold and silicon dioxide surfaces. To validate the result, atomic force microscopy (AFM, Bruker Multimode 8) was used to compare surface roughness between gold and silicon dioxide surface, i.e. the top surface of Au electrodes and the surface between nano-gap Au electrodes. These AFM surface roughness results provides a direct evidence of above selective immobilization processes (Wang et al., 2012; Singh et al., 2014). Fig. 5(a) and (b) shows the AFM images of before-immobilization SiO_2 gap surface (Ori-Gap) and Au electrode surface (Ori-Gold). Fig. 5(c) and (d) shows the AFM images of after-immobilization SiO_2 gap surface (Ab-Gap) and Au electrode surface (Ab-Gold). Fig. 5(e) provides quantitative surface-roughness results obtained from AFM images. From these image results, the height between SiO_2 surface and Au top surface is 30 nm as expected in our device design. Before immobilization processes, the surface roughness (R_{ms}) of Au and SiO_2 surface are 2.26 nm and 0.806 nm, respectively. After immobilization processes, the surface roughness of Au surface (R_{ms}=2.16 nm) is similar as that before immobilization processes. On the other hand, the surface roughness of SiO_2 is 4.96 nm. Based on previous fluorescent and surface-roughness results, the immobilization protocol has a good immobilized selectivity between SiO_2 and Au surfaces. It should be noted that there are some non-specific binding on the top of gold electrodes. Since both fluorescence and AFM results show that the non-specific binding molecules are much less than the cross-linked molecules, it shows non-specific binding antibody cannot form monolayer on the gold surface. Therefore, the sensing mechanism can be shown that it is different from the tradition capacitive biosensor which needs to form dense monolayer on the gold for detection.

3.3. cTnT measurement

In biomolecular detection experiments, cardiac troponin T (cTnT) is employed because it is an important biomarker to detect acute heart failure. In addition, cTnT is also a useful biomarker in prognostic stratification of myocyte injury patients (Lindahl et al., 2000; Aviles et al., 2002; Apple et al., 2005). To examine sensing selectivity of the developed nano-gap biosensor, in experiments, 10 μg/ml bovine serum albumin (BSA) is introduced as an interference background protein. Fig. 6(a) and (b) shows CV measurements of 3 min after 10 μg/ml BSA injection, 28 min after 10 μg/ml BSA injection, and 3 min after 1 μg/ml cTnT antigen injection. In Fig. 6(b), the standard error of capacitance variance in PBS buffer is 2.7%. And this result also demonstrates the non-specific binding effect of 3-min and 28-min BSA incubations, which induces $8 \pm 1.7\%$ capacitance variance in 28-min incubations. After 28-min BSA incubations, the capacitance variance induced by BSA becomes saturated. At the same time, 1 μg/ml cTnT with 3-min incubation leads to a capacitance variance ratio of 22%. These results indicate that the capacitance shifting ratio of BSA, i.e. non-specific binding, is much less than that of cTnT specific binding. It demonstrates the developed device has a good selectivity. In order to limit the non-specific binding and increase the sensitivity of cTnT, we chooses 3 min for the following experiment because it is sufficient for cTnT binding while the non-specific binding interference remains unobvious. For sensitivity tests, 10 μg/ml BSA is mixed with different concentration of cTnT antigen to be testing samples. Fig. 6(c) shows the device has the capability to measure different concentration of cTnT.

Fig. 6(d) summarizes capacitance variance results in different concentration of cTnT. The blank testing curve was measured by

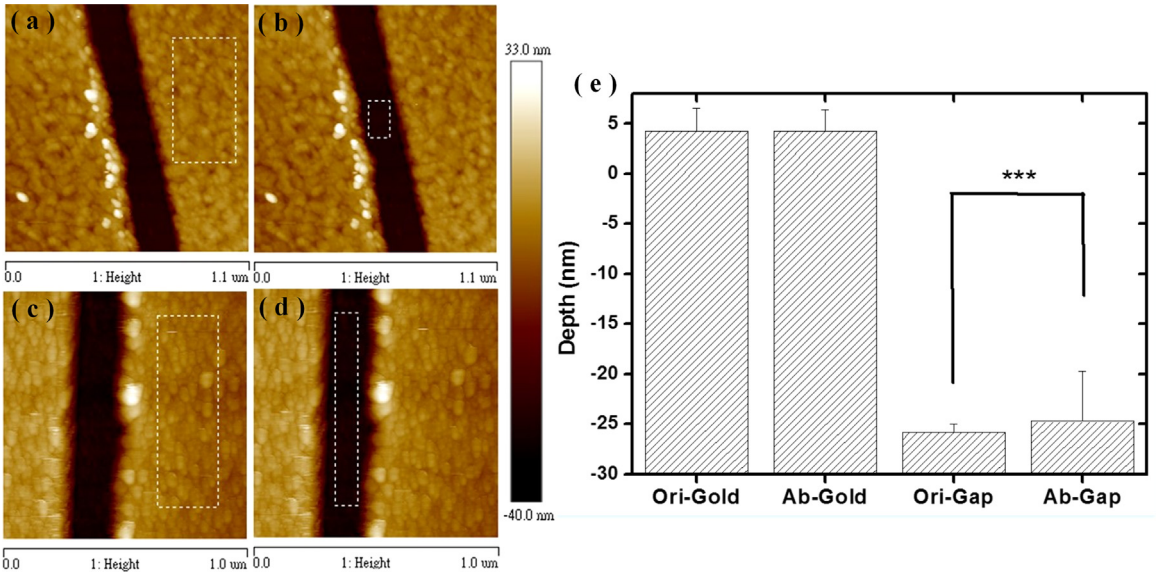

Fig. 5. AFM image of the nano-gap before and after antibody immobilization. (a) Ori-Gold. (b) Ori-Gap. (c) Ab-Gold. (d) Ab-gap. (e) The surface roughness and height results are sampled from the square (dash line) in (a)–(d).

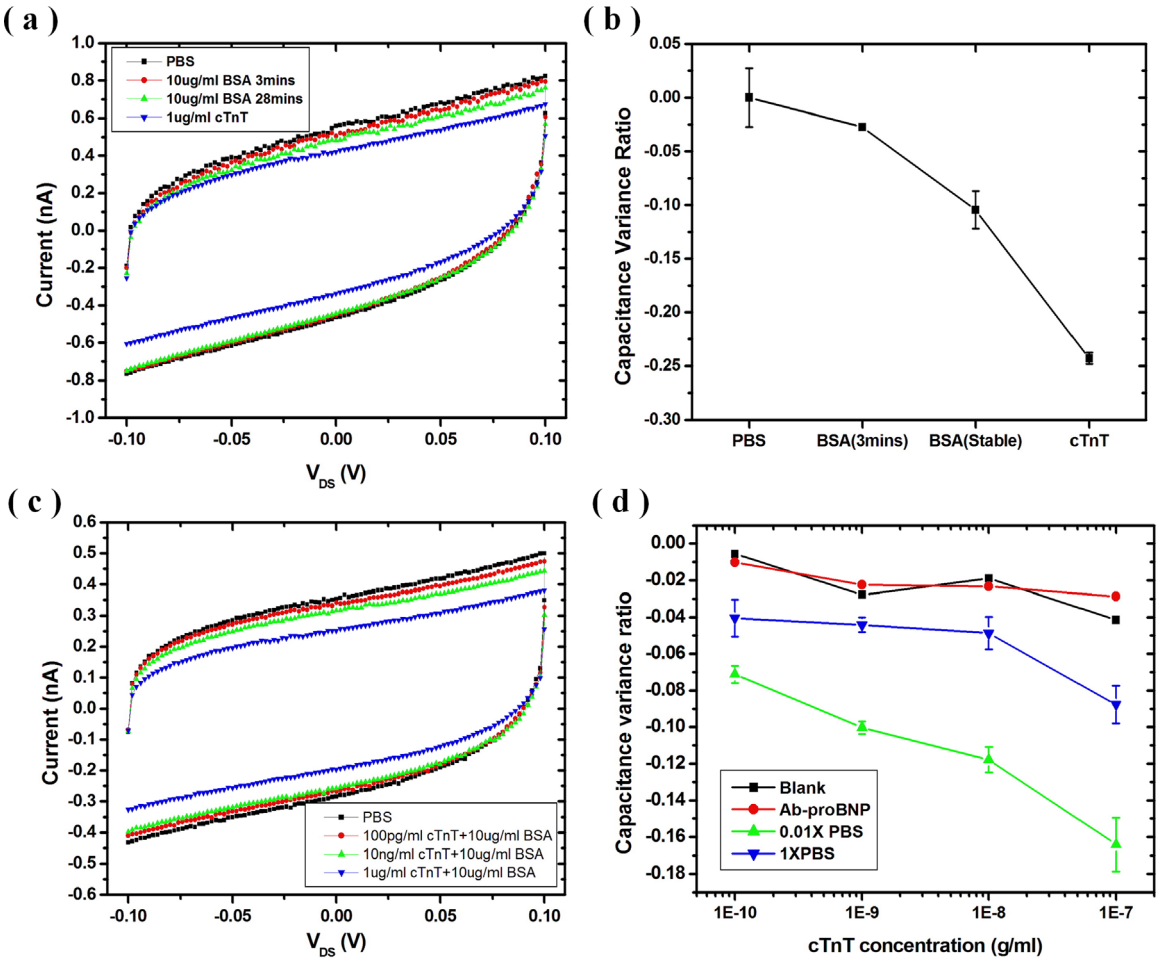

Fig. 6. Fig. 6 (a) The selectivity result measured by cyclic voltammetry and the square(black) ,circle (red), triangle (green), and reversed triangle (blue) curves represent the serial response of the initial state, 10ug/ml BSA injected for 3 minutes, 10ug/ml BSA injected till stable status (28 minutes), and 1ug/ml cTnT injected, respectively. (b) The capacitance variance ratio from Figure 5(a). (c) The sensitivity result measured by CV measurement at different cTnT concentration with 10ug/ml BSA as background. The square(black) ,circle (red), triangle (green), and reversed triangle (blue) curves represent the serial response of the initial state (PBS), 100pg/ml cTnT, 10ng/ml cTnT, and 1ug/ml cTnT, respectively. (d) The capacitance variance ratio. The blank line (black square) represents the result from bare gold without treatment. The Ab-proBNP (red circle) represents the result by using proBNP antibody to detect cTnT. 0.01XPBS (green triangle) and 1XPBS (blue reversed triangle) represent the results measured under 0.01XPBS and 1XPBS buffer solution.

devices without the cTnT antibody cross-link step in 0.01X diluted PBS buffer. The Ab-proBNP testing curve was obtained by devices with the proBNP antibody cross-link step. This was used to demonstrate non-specific binding effect, e.g. cTnT antigen with a non-related antibody. This non-specific binding result is similar to the blank test. It also indicates the non-specific binding would induce a capacitance variance ratio less than 5%. Therefore, 5% capacitance variance ratio can be set as the background noise in biomolecular sensing experiments.

In Fig. 6(d), it also demonstrates an ionic strength effect of the developed device. According to EDL theory (Gouy-Chapman model), the Debye length is inversely proportional to the square root of the ionic strength. In other words, buffers with different ionic strengths affect measurement results of the proposed devices. To examine this characteristics, the cTnT detection with different ionic strength buffers, i.e. non-diluted PBS (1X PBS) and PBS diluted with DI water by 100 v/v (0.01X PBS), can be shown in Fig. 6(d). In 0.01X PBS, the detectable range for cTnT is examined from 100 pg/ml to 100 ng/ml and the limit of detection is less than 100 pg/ml. In 1X PBS buffer, on the other hand, the detectable range of the device is above 10 ng/ml. Because of the higher ion concentration of 1X PBS than that of 0.01 PBS, the surface charge variance induced by cTnT binding might be overwhelmed by high ion concentration in 1X PBS. As a consequence, the proposed nano-gap incremental capacitance measurement has better detection limit in diluted PBS buffer than that in non-diluted PBS buffer. This result also reveals the sensing characteristics of the developed method correlates to the properties of electrical double layer. For cTnT clinical applications, two different concentrations are usually used as cut-off levels, i.e. concentration level < 10 pg/ml are considered as 'Normal'; concentration levels between 10 and 35 pg/ml are considered as 'likely pathological'; and concentration level > 35 pg/ml are considered as 'pathological' (Twerenbold et al., 2012; Hammerer-Lercher et al., 2013). Therefore, in our device, the demonstrated detection concentration (100 pg/ml) is slightly higher than the clinical decision cut-off region (35 pg/ml). Based on previous discussions, this newly developed biomolecular sensing mechanism can be further improved by decreasing the sensing buffer concentration to enlarge the Debye length or shorten the gap length between electrodes.

In previous cTnT sensing experiments, it should be noted that the capacitance variance ratio is negative. This shows that cTnT binding decreases the surface potential in nano-gap devices, i.e. the number of surface charges reduces as cTnT binding occurs. To verify the phenomenon, two-dimensional electrophoresis is used to check the isoelectric pointe (pI) of cTnT and its antibody (as

shown in Supporting information, Fig. S2). The electrophoresis result indicates the pI value of cTnT is around 6 and the pI value of cTnT antibody light chain is around 8. In other words, cTnT is negative charged and cTnT antibody is positive charged in the experimental PBS buffer (pH=7.2). As cTnT binds with cTnT antibody, therefore, molecular net charges would be compensated to each other and the charged surface is neutralized. This leads to a decrease of surface potential and causes negative incremental capacitance variance. This also agrees with our previous experiments by modifying charged surface functional groups. As mentioned previously, it should be noted that the temporal responses of these capacitance variance measurements can be obtained. As a consequence, the temporal detection of chemicals or biological pairs with different disassociate constant can be also characterized by the proposed nano-gap device and method. It provides a useful tool for avidity selection in clinical examinations.

4. Conclusions

In conclusion, we have demonstrated a novel surface-potential-variation measurement method by using a planar nano-gap device. Modulations of surface potential affect electric double layer and capacitance between nano-gap electrodes. In this work, this effect is verified by immobilizing different charged functional groups and the correlation between the surface potential and incremental-capacitance variance is also demonstrated. Based on this effect, the application for cTnT biomarker detection is implemented. The detectable range for cTnT measurement is from 100 pg/ml to 10 μg/ml and the detection limit is less than 100 pg/ml in 0.01X PBS buffer, though the detection limit is slightly higher than the clinical decision cut-off region (35 pg/ml). In addition, it is experimentally demonstrated that the low ion concentration buffer has better detection characteristics than high ion concentration buffer does. Based on this work, the incremental double-layer capacitance of a planar nano-gap structure can provide a simple and reliable method for surface potential monitoring and can be used for different chemical and clinical examinations.

Acknowledgments

The authors would like to thank the financial supporting from Ministry of Science and Technology (MOST) in Taiwan (104-2221-E-002-164-MY2 and 104-2628-E-002-014-MY3) and National Taiwan University (104R890943).

Appendix A. Supplementary material

Supplementary data associated with this article can be found in the online version at http://dx.doi.org/10.1016/j.bios.2015.12.105.

Reference

Apple, F.S., Wu, A.H.B., Mair, J., Ravkilde, J., Panteghini, M., Tate, J., Pagani, F., Christenson, R.H., Mocker, M., Danne, O., Jaffe, A.S., 2005. Clin. Chem. 51, 810–824.
Aviles, R.J., Askari, A.T., Lindahl, B., Wallentin, L., Jia, G., Ohman, E.M., Mahaffey, K. W., Newby, L.K., Califf, R.M., Simoons, M.L., Topol, E.J., Berger, P., Lauer, M.S., 2002. New. Engl. J. Med. 346, 2047–2052.
Bard, A.J., Faulkner, L.R., 2001. Electrochemical Methods, Fundamentals and Applications, 2nd ed. John Wiley & Sons, Inc., New York.
Berdat, D., Rodríguez, A.C.M., Herrera, F., Gijs, M.A.M., 2008. Lab Chip 8, 302–308.
Bocquet, L., Charlaix, E., 2010. Chem. Soc. Rev. 39 (3), 1073–1095.
Chapman, D.L., 1913. Philos. Mag. 25, 475.
Christenson, R.H., Duh, S.-H., Newby, L.K., Ohman, E.M., Califf, R.M., Granger, C.B., Peck, S., Pieper, K.S., Armstrong, P.W., Katus, H.A., Topol, E.J., 1998. Clin. Chem. 44, 494–501.
Evans, D.F., Wennerström, H., 1999. The Colloidal Domain: Where Physics, Chemistry, Biology, and Technology Meet. Wiley–VCH, New York.
Gu, Y.G., Li, D.Q., 2000. J. Colloid Interface Sci. 226, 328–339.
Hammerer-Lercher, A., Ploner, T., Neururer, S., Schratzberger, P., Griesmacher, A., Pachinger, O., Mair, J., 2013. J. Am. Heart Assoc. 2, e000204.
Harris, L.J., Larson, S.B., Hasel, K.W., McPherson, A., 1997. Biochem 36, 1581–1597.
Ohshima, H., Kondo, T., 1990. J. Colloid Interface Sci. 135, 443–448.
Itoh, Y., Kim, B., Gearba, R.I., Termblay, N.J., Pindak, R., Matsuo, Y., Nakamura, E., Nuckolls, C., 2011. Chem. Mater. 23, 970–975.
Jacobs, H.O., Leuchtmann, P., Homan, O.H., Stemmer, A., 1998. J. Appl. Phys. 84, 1168–1173.
Kirby, B.J., Hasselbrink, E.F., 2004. Electrophoresis 25, 187–202.
Lasne, F., 2001. J. Immunol. Methods 253, 125–131.
Leroy, P., Tournassat, C., Bizi, M., 2011. J. Colloid Interface Sci. 356 (2), 442–453.
Lindahl, B., Toss, H., Siegbahn, A., Venge, P., Wallentin, L., 2000. New. Engl. J. Med. 343, 1139–1147.
Mirsky, V.M., Riepl, M., Wolfbeis, O.S., 1997. Biosens. Bioelectron. 12, 977–989.
Radke, S.M., Alocilja, E.C., 2005. Biosens. Bioelectron. 20, 1662–1667.
Salmio, H., Brühwiler, D., 2007. J. Phys. Chem. C 111, 923–929.
Simon, P., Gogotsi, Y., 2008. Nat. Mater. 7, 845–854.
Singh, R., Sharma, A., Hong, S., Jang, J., 2014. Analyst 139, 5415–5421.
Siria, A., Poncharal, P., Biance, A.L., Fulcrand, R., Blase, X., Purcell, S.T., Bocquet, L., 2013. Nature 494 (7438), 455–458.
Taylor, D.M., Morgan, H., Silva, C.D., 1991a. J. Phys. D: Appl. Phys. 24, 1443–1450.
Taylor, R.F., Marenchic, I.G., Spencer, R.H., 1991b. Anal. Chim. Acta 249, 67–70.
Twerenbold, R., Jaffe, A., Reichlin, T., Reiter, M., Mueller, C., 2012. Eur. Heart J. 33, 579–586.
Valera, E., Ramón-Azcón, J., Rodríguez, Á., Castañer, L.M., Sanchez, F.J., Macro, M.P., 2007. Sens. Actuators B – Chem. 125, 526–537.
Wang, H., Pilon, L., 2012. Electrochim. Acta 63, 55–63.
Wang, S., Esfahani, M., Gurkan, U.A., Inci, F., Kuritzkes, D.R., Demirci, U., 2012. Lab. Chip 12, 1508–1515.
Winter, M., Brodd, R.J., 2004. Chem. Rev. 104, 4245–4269.
Yang, L.J., Li, Y.B., Erf, G.F., 2004. Anal. Chem. 76, 1107–1113.